2013 IEEE/RSJ International Conference on
Intelligent Robots and Systems (IROS)
November 3-7, 2013. Tokyo, Japan

Stabilization of a Flying Vehicle on a Taut Tether using Inertial Sensing

Sergei Lupashin and Raffaello D'Andrea

***Abstract*— Given a hover-capable flying vehicle attached to a fixed point by a taut tether, we present a novel method to recover the vehicle's relative position and absolute orientation. The proposed method requires only on-board inertial sensors, and indirectly measures the string force, enabling the additional use of the tether as a physical user interaction medium. We present the vertical-plane dynamics of such a system and the localization approach, discuss sensitivity issues, and implement an estimator and controller based on the presented model. We demonstrate the method experimentally on a tethered quadrocopter in the Flying Machine Arena, using both a vertical-plane-constrained vehicle and in 3D.**

I. Introduction

Small hover-capable unmanned aerial vehicles (UAVs) are being used extensively in research and are beginning to be used in civil applications such as aerial photography and inspection. Currently such vehicles rely either on external localization systems like GPS or require external control. More recently, proof-of-concept autonomous vision-guided flight has been demonstrated [1], [2], with sophisticated machine vision and estimation algorithms providing the required localization.

As a result, while small UAVs are capable of providing unique sensing perspectives in numerous situations, in realistic settings they are virtually unusable by non-experts. A high level of situational awareness is required to prevent loss of control and expert training is necessary to recover the vehicle from non-ideal situations. The lack of resilient, low-cost, effective localization and interaction methods remains a composite barrier for the wider adoption of such devices. The localization/interaction barrier is further amplified by the variety and challenging nature of immediate applications such as search and rescue or disaster recovery.

In this work we propose a new stabilization approach based on the analysis of the dynamics of a hover-capable UAV attached to the ground via a taut tether. While adding some restrictions to the operational scenarios of the UAV, we show that a taut tether provides both a unique new modality for stabilizing the vehicle and creates a novel user-vehicle interaction method. In addition, as recent commercial developments such as [3] have shown, a tether provides further potential advantages beyond the scope of this work, as a power transmission system or as a reliable, high-bandwidth electro-optical communication channel.

Taut tethers in robotics have been used for aerial installations for energy generation [4], [5]. The dynamics of a robot swinging under a support point on the end of a tether were described and a controller was proposed in [6]. The use of tethered flight has also been proposed for operating in proximity of ships, such as for landing or taking off from a vessel in rough seas [7], [8]. In addition, tethers have been used in ground robotics, such as on the proposed Axel tethered rover for planetary exploration [9]. Tethers have also been used extensively in the context of kites and balloons used for aerial photography[10].

In this work we consider a hover-capable UAV such as a quadrocopter, capable of following body rate commands and producing a collective thrust, attached by a taut tether to a fixed or slowly moving ground point (see Fig. 1). The goal is to find the state of the vehicle using only on-board inertial sensors and to use that information in feedback to be able to control the vehicle to a desired position.

We begin by describing the first-principles planar dynamics of the system in Section II. We then discuss how these dynamics and minimal sensing in the form of on-board inertial sensors can be exploited to localize the vehicle in Section III. We improve on that localization approach by describing a full estimator in Section IV. Given the estimated state of the vehicle and the system model, we describe a

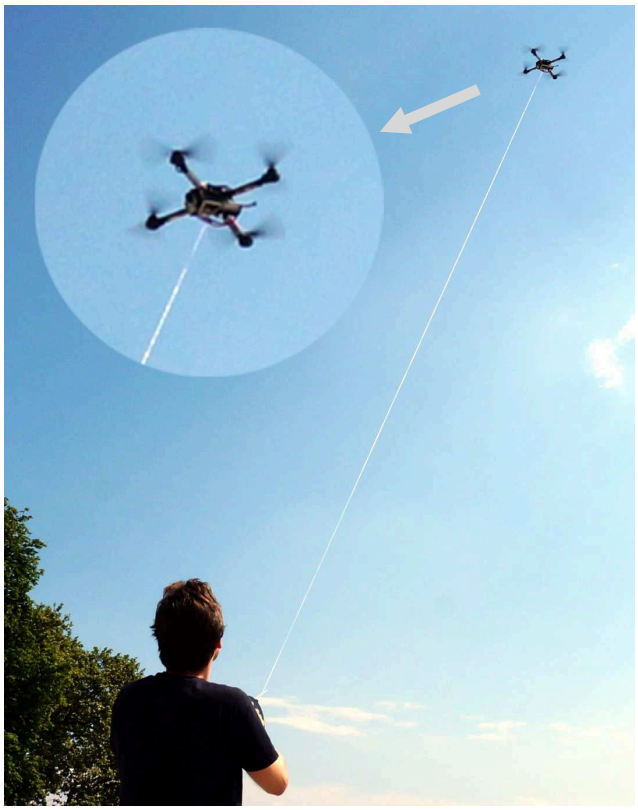

Fig. 1. A tethered self-propelled flying vehicle operated by a person.

The authors are with the Institute for Dynamic Systems and Control (IDSC), ETH Zurich, Sonneggstr. 3, 8092 Zurich, Switzerland {sergeil, rdandrea}@ethz.ch.

978-1-4673-6358-7/13/$31.00 ©2013 IEEE

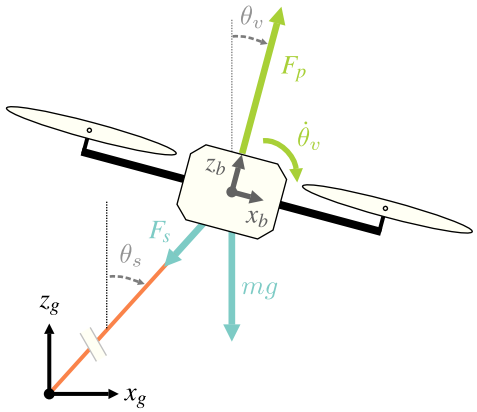

Fig. 2. Close-up of the tethered flying vehicle highlighting the relevant variables and forces (F_p, F_s and mg). The inputs to the system are shown in green: the collective thrust force F_p and the desired angular rate $\dot{\theta}_v$.

control scheme in Section V and examine local stability in Section VI. Finally, we show preliminary results and discuss performance in Section VII before giving a brief conclusion and outlook in Section VIII.

II. System Modeling

We examine a vertical-plane simplification of the system: Consider a flying vehicle attached by a tether to a fixed point on the ground. The vehicle has mass m and the tether is taut and of fixed length l. The mass of the tether is negligible and it is straight. It is attached to the center of mass of the vehicle on one end and to the global coordinate frame origin on the other. We assume that aerodynamic effects are negligible.

Our goal is to recover how the local coordinate system (x_b, z_b) relates to the global reference frame (x_g, z_g), which, given a known tether length l, corresponds to recovering the two angles θ_v and θ_s. A depiction of the forces and variables involved is shown in Fig. 2.

From first principles, the translational dynamics are

$$\begin{aligned} m\ddot{x}_b &= mg\sin\theta_v - F_s\sin(\theta_s - \theta_v) \\ m\ddot{z}_b &= F_p - mg\cos\theta_v - F_s\cos(\theta_s - \theta_v) \end{aligned} \tag{1}$$

where g is acceleration due to gravity, and F_p, F_s are the propeller and tether tension forces, respectively.

From here on, we omit the mass of the vehicle in further analysis and assume that F_p and F_s are normalized by m.

Since the tether is kept taut, F_s must equal the sum of all the other forces in the direction of the tether:

$$F_s = F_p\cos(\theta_s - \theta_v) - g\cos\theta_s + l\dot{\theta}_s^2 \tag{2}$$

The dynamics of θ_s are governed by the relevant components of the forces in Eqn. 1:

$$\ddot{\theta}_s = \frac{g\sin\theta_s - F_p\sin(\theta_s - \theta_v)}{l} \tag{3}$$

III. Minimal Localization

Given the above system dynamics, we show that only on-board inertial sensors can be used to recover θ_s' and θ_v', the approximate values of θ_s and θ_v, respectively. While more sophisticated estimation algorithms may be used to recover the state (e.g. see Section IV), this approach provides a light-weight, understandable, minimal way to observe the two angles. In addition, examining the localization procedure closely reveals how this measurement scheme performs under non-ideal conditions and provides guidelines for optimal operating points of the system.

An accelerometer measures the acceleration effected by the composition of all the non-gravitational forces acting on the accelerometer [11]. In other words, an on-board accelerometer measures the effects of all the forces in Eqn. 1, minus the acceleration corresponding to gravity: the accelerometer measurements a_x, a_z, taken with respect to the body axes x_b, z_b are

$$\begin{aligned} a_x &= -F_s\sin(\theta_s - \theta_v) \\ a_z &= F_p - F_s\cos(\theta_s - \theta_v) \end{aligned} \tag{4}$$

We assume the collective thrust F_p is nominally set to some commanded value F_p^*, high enough to keep the tether taut. From Eqn. 4 we solve for the measured tether force F_s':

$$F_s' = \sqrt{a_x^2 + (a_z - F_p^*)^2} \tag{5}$$

Note that, under ideal conditions, if the tether is not taut $a_x = 0$ and $a_z = F_p^*$, leading to $F_s' = 0$ from the above calculation. In the presence of sensor noise and disturbances, a threshold, $F_s' < \epsilon$, may be used to detect if the tether is taut at a given time.

Assuming that the centripetal force is negligible, we solve Eqn. 2 and Eqn. 4 for angle measurements θ_s' and θ_v':

$$\cos\theta_s' = \frac{F_p^*(F_p^* - a_z)/F_s' - F_s'}{g} \tag{6}$$

$$\theta_v' = \theta_s' - \sin^{-1}(-a_x/F_s') \tag{7}$$

Note that the sign of θ_s', and hence the value of θ_v', are ambiguous. This is resolved by using on-board gyros to predict a prior for θ_v' and picking the closer corresponding θ_s' as the update value.

As a result of the $\sin^{-1}$ and $\cos^{-1}$, there are two conditions that must be satisfied to make the observation:

$$\begin{aligned} |F_p^*\cos(\theta_s - \theta_v) - F_s'| &\le g \\ |a_x/F_s'| &\le 1 \end{aligned} \tag{8}$$

given the previous assumptions, both conditions are ideally always satisfied from Eqn. 2 and Eqn. 4. In presence of sensor noise, unmodeled effects and disturbances, special care must be taken to filter out unusable measurements.

A. Sensitivity Analysis

The equations for recovering the state of the vehicle are nonlinear and are not always well-behaved. For example, θ_s is practically unrecoverable around 0, since only $\cos\theta_s$ is observed directly. We performed a series of Monte-Carlo simulations to understand how the proposed state observation approach performs under different conditions. As the calculation for the tether force F_s is straightforward, we performed a sensitivity analysis only for θ_v' and θ_s'.

For each of these tests, we examined how the localization approach functioned for static operating points ($\ddot{\theta}_s = 0$) at

various set points $\check{\theta}_s$. For a given $\check{\theta}_s$, the attitude of the vehicle $\theta_v = \check{\theta}_v$ required for the vehicle to remain static is derived by setting $\ddot{\theta}_s = 0$ in Eqn. 3:

$$\check{\theta}_v = \check{\theta}_s - \sin^{-1}\left(\frac{g \sin \check{\theta}_s}{F_p}\right) \tag{9}$$

1) Sensitivity to Unbiased Gaussian Noise: Noise sampled from zero-bias Gaussian distributions $\mathcal{N}(0, \sigma^2)$ were applied to the ideal accelerometer measurements (see Fig. 3). The standard deviation σ of the distributions was set to $0.2\,\mathrm{m\,s^{-2}}$, representative of accelerometer noise on a well-maintained, vibration-isolated hovering quadrocopter [12]. The analysis shows that higher θ_s set point values provide more robust observations, with significant measurement bias for $\theta_s < 20°$. As a result of the sensor noise some measurements violated the constraints described in Eqn. 8, and were not used for measurements, leading to additional mean measurement bias near $\theta_s = 0$.

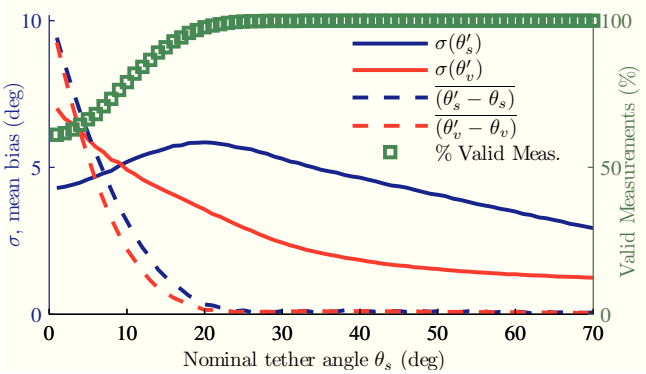

Fig. 3. Representative effect of Gaussian zero-bias sensor noise on state observation. Each point represents either the standard deviation ($\sigma(\cdot)$) or the mean bias ($\overline{\theta' - \theta_\cdot}$) calculated from 50,000 simulated measurements. Sensor noise was sampled from $\mathcal{N}(0, \sigma^2_{x,z})$, where σ_x and σ_z were set to $0.2\,\mathrm{m\,s^{-2}}$. Thrust F_p was set to $12\,\mathrm{m\,s^{-2}}$.

2) Sensitivity to Collective Thrust Mismatch: Note that in the analysis we assumed F_p is known and equal to the input F_p^* to the vehicle. The actual thrust produced by the propellers typically does not match the ideal value: for example, actual thrust gradually decreases over time due to propeller wear. We repeated the above sensitivity analysis with $F_p^* = 12\,\mathrm{m\,s^{-2}} = F_p + 0.5\,\mathrm{m\,s^{-2}}$ (Fig. 4). The localization clearly performs best for larger values of θ_s, specifically $\theta_s > 20°$; in addition to the previous issues of observation bias, the effect of $F_p < F_p^*$ results in practically no usable localization observations near $\theta_s = 0$.

3) Centripetal Force: We made the assumption that the centripetal force is negligible in order to derive Eqn. 6. If the centripetal force is indeed substantial then both θ'_s and θ'_v will be offset from their true values. We examine how well this approximation holds for several realistic scenarios in Fig. 5. Larger values of θ_s are once again better behaved, with errors arising from this approximation scaling much worse with $\dot{\theta}_s$ than with l. Practically, this means that the approximation may be a problem at smaller tether lengths, as at larger values of l the translational speeds equivalent

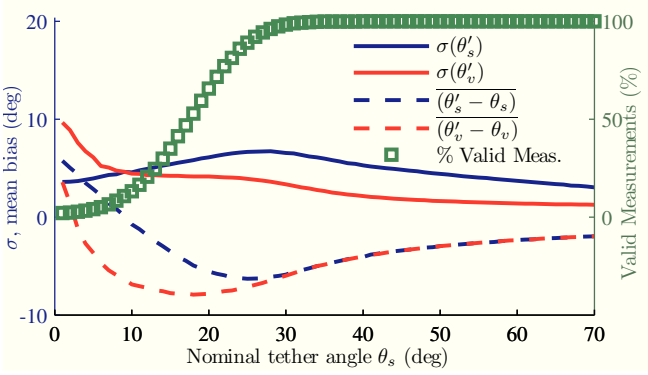

Fig. 4. Observation/measurement sensitivity analysis as in Fig. 3, but with $F_p = 11.5\,\mathrm{m\,s^{-2}} = F_p^* - 0.5\,\mathrm{m\,s^{-2}}$. Note that near $\theta_s = 0$ the minimal localization measurement conditions (Eqn. 8) are violated by a majority or all the measurements, resulting in a significant mean measurement bias.

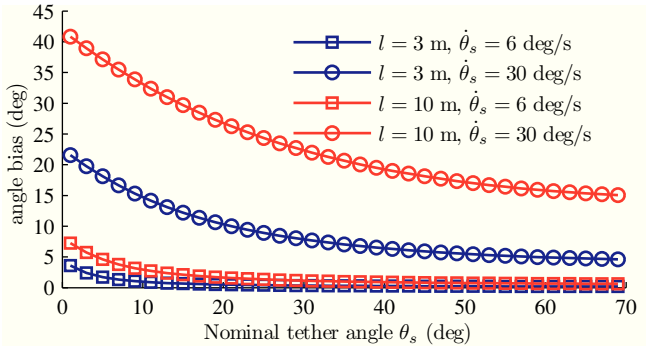

Fig. 5. Sensitivity of the minimal localization scheme to the negligible centripetal force assumption. The system parameters are as in Fig. 3. Note that the approximation is much more sensitive to $\dot{\theta}_s$ than to l, since centripetal angle is quadratically related to $\dot{\theta}_s$ and linear in l.

to significant $\dot{\theta}_s$ are quickly not practical (e.g. drag, other effects become significant).

Since our primary objective is to stabilize at a given θ_s, rather than dynamically change the angle, the magnitude of $\dot{\theta}_s$ should remain relatively small, preventing significant localization errors due to this approximation. As a further improvement, we may use the current estimate of $\dot{\theta}_s$, if available, to approximately cancel out the effect of the centripetal force on the measurement.

IV. Estimation

Given the measurements a_x, a_z and the dynamics of the system, we want to produce an estimate of the current state of the system, $\hat{\mathbf{x}}$, to enable us to control the system.

We implement an Unscented Kalman Filter (UKF) [13], which avoids requiring differentiating or analytically approximating the system dynamics and measurement equations, and instead uses a small number of strategically picked "sigma points" to perform the filtering, similar to a particle filter. The UKF requires noise models for the process and the measurements, the dynamics equations of the process, and a mapping from a given state to the respective measurement.

We define the estimated state at time instant k as:

$$\hat{\mathbf{x}}^k = \left(\hat{\theta}_s^k, \hat{\dot{\theta}}_s^k, \hat{\theta}_v^k\right) \tag{10}$$

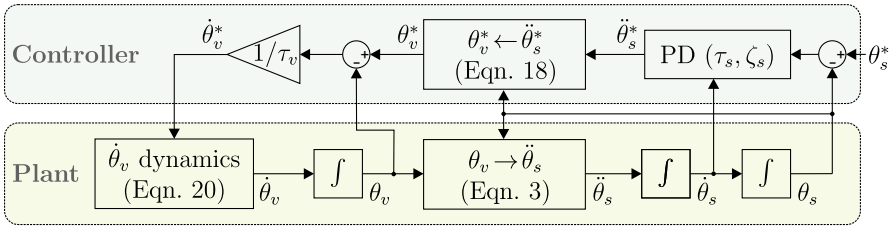

Fig. 6. Layout of the closed-loop tethered vehicle system, including the plant (bottom) and the proposed controller (top). The estimator and accelerometers are omitted for clarity – all state variables used by the controller are estimated, as it has no access to the true state of the system.

The process is modeled using the discrete Wiener process acceleration model [14] with a nonlinear prediction step,

$$\mathbf{x}^{k+1} = \mathbf{x}^k + \mathrm{RK}_4(f(\mathbf{x}^k)) + \Gamma v^k \tag{11}$$

where $\mathrm{RK}_4(\cdot)$ is the fourth-order Runge-Kutta numeric integration method, v^k is an acceleration increment at the kth sampling period, assumed to be a zero-mean white sequence, Γ is the noise gain discussed below, and $f(\cdot)$ is the nonlinear dynamics from Section II,

$$f(\mathbf{x}^k) = \begin{bmatrix} \hat{\dot{\theta}}_s^k \\ (g \sin \hat{\theta}_s^k - F_p \sin(\hat{\theta}_s^k - \hat{\theta}_v^k))/l \\ \omega^k \end{bmatrix}, \tag{12}$$

where ω^k is the on-board rate gyro measurement at time k.

The noise gain Γ corresponds to that of a discrete Wiener process acceleration model, but with a nominal-set-point linearized change of variables from $\hat{\dot{\theta}}_s$ to $\hat{\theta}_v$:

$$\Gamma = \begin{bmatrix} T^2/2 & T & \partial\theta_v/\partial\ddot{\theta}_s\Big|_{\check{\theta}_s, \check{\theta}_v} \end{bmatrix}^T, \tag{13}$$

where T is the sample time and the partial derivative is computed from Eqn. 3:

$$\frac{\partial \theta_v}{\partial \ddot{\theta}_s}\bigg|_{\check{\theta}_s, \check{\theta}_v} = \frac{l}{F_p \cos(\check{\theta}_s - \check{\theta}_v)} \tag{14}$$

This corresponds to appropriate integral of the the acceleration v^k per sample time T, with the increment in $\ddot{\theta}_s$ approximately transformed into an increment in θ_v.

The resulting covariance of the process noise is [14]

$$\mathbf{Q} = \Gamma \sigma_p^2 \Gamma^T, \tag{15}$$

where σ_p is a tuning parameter and should be on the order of magnitude of the maximum unmodeled acceleration of θ_s in one time increment. For the experiments presented in this work, $\sigma_p = 0.4$.

The measurement noise covariance, $\mathbf{R}$, was calculated from experimental measurement data. For the experiments presented in this work,

$$\mathbf{R} = \begin{bmatrix} 0.31 & 0.157 \\ 0.157 & 1.105 \end{bmatrix} \tag{16}$$

UKF update steps are only performed when a valid measurement is detected, i.e. $\sqrt{a_x^2 + (a_z - F_p^*)^2} > \epsilon$ as per Section III. If this condition fails, a "dead-reckoning" update step is executed. The filter is initialized using the first valid observation, using the state produced by the minimal localization method given in Section III.

V. Control

Based on the state estimate $(\hat{\theta}_s, \hat{\dot{\theta}}_s, \hat{\theta}_v)$ produced in Section IV, we design a controller to stabilize the system at a given set point $\check{\theta}_s$. A diagram of the resulting closed-loop system is shown in Fig. 6.

The vehicle accepts as input a collective thrust command F_p^* and a desired body rate $\dot{\theta}_v^*$. We set F_p^* to a constant value, sufficiently high such that the tether is kept taut.

To find $\dot{\theta}_v^*$, we first use a proportional-derivative controller to find a desired tether angle acceleration $\ddot{\theta}_s^*$:

$$\ddot{\theta}_s^* = \frac{1}{\tau_s^2}(\check{\theta}_s - \hat{\theta}_s) - \frac{2\zeta_s}{\tau_s}\hat{\dot{\theta}}_s \tag{17}$$

where τ_s is the desired time constant of the closed-loop system and ζ_s is the desired damping ratio.

We then transform $\ddot{\theta}_s^*$ to a desired vehicle angle by feedback linearization, using the inverse of the relevant system dynamics (Eqn. 3):

$$\theta_v^* = \hat{\theta}_s - \sin^{-1}\left(\frac{g \sin \hat{\theta}_s - l\ddot{\theta}_s^*}{F_p^*}\right) \tag{18}$$

Finally, we use another proportional controller to calculate the desired vehicle angular rotation:

$$\dot{\theta}_v^* = \frac{1}{\tau_v}(\theta_v^* - \hat{\theta}_v) \tag{19}$$

where τ_v is the desired closed-system time constant for the vehicle angular dynamics.

We set ζ_s to 0.6 for good performance and minimal overshoot. The remaining two control parameters, τ_s and τ_v, were tuned experimentally to $0.6\,\mathrm{s}$ and $0.16\,\mathrm{s}$, respectively.

VI. Local Stability Analysis

The estimator describe in Section IV is independent of the controller described in Section V. Therefore, for the purpose of proving local stability, by the separation principle [15], we may treat the estimator and the controller separately, first showing stability for the UKF and then showing stability for the controller given perfect estimated state information, $\hat{\mathbf{x}} = \mathbf{x}$.

A. Estimator Stability

For local (linear) analysis, the UKF update equations reduce to the standard Kalman filter update step, which is stable if the estimator state variables are observable from the measurements [14]. The UKF is known to be locally stable for estimating the state of nonlinear systems given

that the filter is correctly initialized (initial state close to true value) and the provided noise models reflect the noise in the actual process/measurements [16]. Given that we initialize the estimator with the minimal localization method presented in Section III, a good initial state estimate is reliably available for properly chosen operating set points.

To show controller stability, we first identify the dynamics of the vehicle following angular rate commands.

B. Vehicle Angle Rate Dynamics

We identified the dynamics of the quadrocopter following angular rate commands as a second-order system by curve-fitting to experimental step response data. The response of the physical system to a step in $\dot{\theta}_v^*$ is shown in Fig. 7. More details about the test setup and the vehicles used is given in Section VII. We observe that the dynamics of $\dot{\theta}_v$ near $\dot{\theta}_v = 0$ are well represented by a second-order system:

$$\ddot{\dot{\theta}}_v = \omega_{vd}^2(\dot{\theta}_v^* - \dot{\theta}_v) - 2\zeta_{vd}\omega_{vd}\ddot{\theta}_v, \tag{20}$$

with $\omega_{vd} = 78.5\,\mathrm{rad\,s^{-1}}$ and damping $\zeta_{vd} = 0.4$.

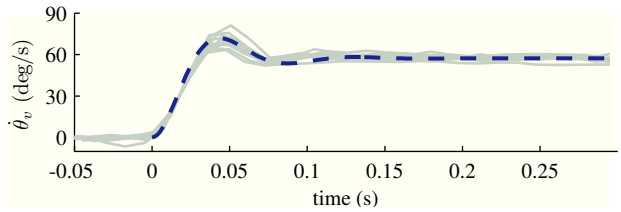

Fig. 7. Step response of a quadrocopter in the Flying Machine Arena to $\dot{\theta}_v^*$, compared to the step response of an ideal second order system with $\omega_{vd} = 78.5\,\mathrm{rad\,s^{-1}}$, $\zeta = .4$ (dashed line). At time 0 s the vehicle was commanded $\dot{\theta}_v^* = 60\,^\circ\,\mathrm{s^{-1}}$. Ten trials are shown.

C. Controller Stability

To show local controller stability, we combine the vehicle angle rate dynamics above with the tether dynamics described in Section II and the controller (Section V) into a closed-loop nonlinear system, and linearize it at various static operating points. For completeness, the analytical linearization of the system dynamics and the controller is provided in the Appendix.

The poles of the closed-loop system linearized at various operating points are shown in Fig. 8. They are stable for all configurations. Furthermore, the two poles corresponding to the dynamics of $\dot{\theta}_v$, are distant from the other poles, highlighting time scale separation between vehicle dynamics and tether/controller dynamics.

$\check{\theta}_s$	10°	50°	90°
$\check{\theta}_v$	1.84°	11.23°	35.17°
	$-28.5\pm70.8i$	$-28.5\pm70.8i$	$-28.5\pm70.8i$
	-3.6	-3.5	-2.8
	$-1.1\pm1.8i$	$-1.1\pm1.8i$	$-1.5\pm1.9i$

Fig. 8. Closed-loop system poles at various set points. The controller parameters were set to $\tau_s = 0.6\,\mathrm{s}$, $\zeta_s = 0.6$, and $\tau_v = 0.18\,\mathrm{s}$. The vehicle angle rate dynamics are as identified in Section II, $\omega_{vd} = 78.5\,\mathrm{rad\,s^{-1}}$, $\zeta_{vd} = 0.4$. Other parameters: $l = 3\,\mathrm{m}$, $F_p^* = 12\,\mathrm{m\,s^{-2}}$.

VII. Results

A. Experimental Setup

The feasibility of the proposed localization and control method was tested in the Flying Machine Arena (FMA) aerial robotics testbed [12]. A small quadrocopter was attached by a 3 m string to a fixed point on the ground or, in later tests, to a tracked object held by a person. The string used is highly inelastic and is very lightweight ($0.9\,\mathrm{g\,m^{-1}}$). The true position and attitude of the vehicle were measured by a high-precision motion capture system. For all experiments, $F_p^* = 12\,\mathrm{m\,s^{-2}}$.

The Flying Machine Arena system was used to constrain the vehicle to the (x_g, z_g) plane using the standard off-board FMA controllers described in [12].

On-board accelerometers measured the accelerations at 800 Hz, filtered by a first-order digital lowpass filter with a time constant of 0.06 s. These filtered measurements were sent to an estimator at 80 Hz, A controller running at 50 Hz used the current estimated state to produce and send control commands (F_s^* and $\dot{\theta}_v^*$) to the vehicle.

B. Tether Torque Compensation

The model presented in Section II assumes that the tether is attached to the center of mass of the vehicle and that it creates no torques on the vehicle. In practice this is impractical; a natural tether attachment point, used in the experiments presented, is a short distance d below the center of mass on the vehicle on (that is, at $z_b = -d$). In this case we assume $d \ll l$ and use the observation F_s' and the current state estimate to calculate an opposing equivalent torque ρ:

$$\rho = -d\gamma F_s' \sin(\hat{\theta}_s - \hat{\theta}_v) \tag{21}$$

where γ is a force to torque conversion factor calculated from the inertial properties of the vehicle.

This torque is then sent as a feed-forward command to the vehicle, resulting in the cancellation of the unwanted torque.

C. Minimal Localization

Results of the minimal localization procedure are shown in Fig. 9. The observed values are noisy but track the true value.

D. Estimation and Closed-Loop Angle Control

Fig. 10 shows a quadrocopter in the FMA attached to a static point on the ground responding to a change in commanded tether angle, θ_s^*. The tether angle controller (Section V) is using the estimated state produced by the UKF (Section IV) to stabilize the vehicle and follow the setpoint.

E. Stabilization with Moving Anchor Point

Further experiments were conducted where the anchor point (the bottom end of the tether) was moved around. An example of such an experiment is shown in Fig. 11. This allows for natural interactive position control, as the vehicle is able to keep station relative to the user.

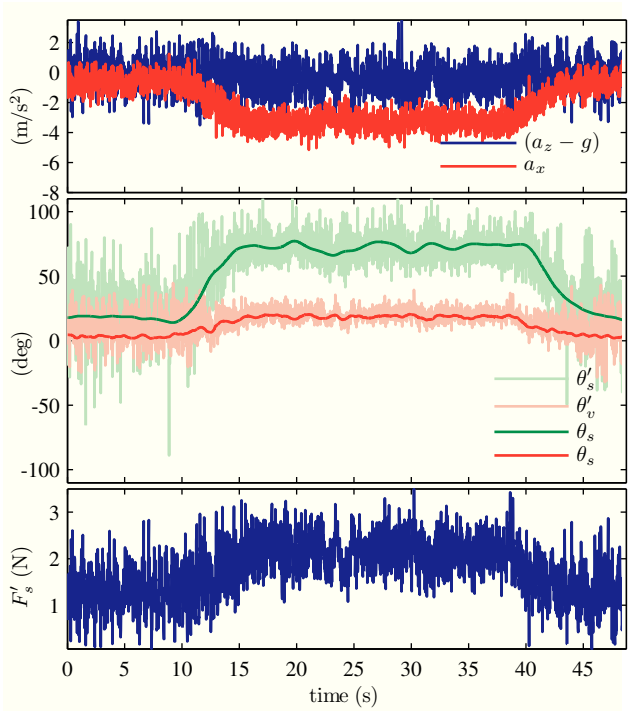

Fig. 9. Accelerometer data and resulting $\theta'_s, \theta'_v, F'_s$ from the minimal localization scheme for a tethered quadrocopter. Ground truth values of the angles, θ_s (green) and θ_v (red) are shown as reference.

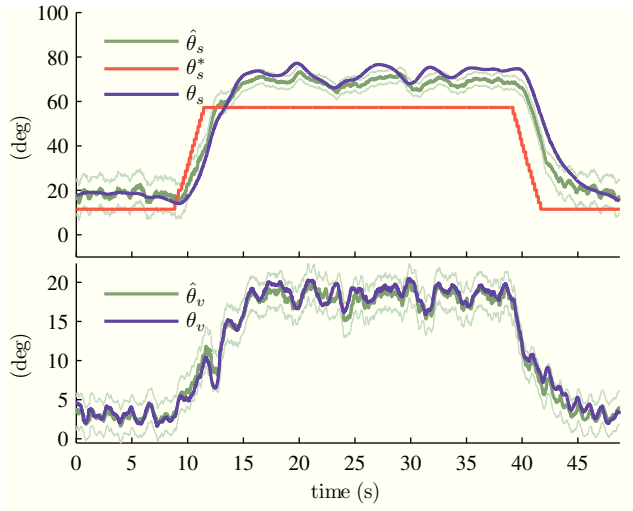

Fig. 10. Commanded, UKF-estimated, and true angles for a vehicle following tether angle commands while tethered to a static anchor point. The mean estimates $\hat{\theta}_s$ and $\hat{\theta}_v$ are plotted against the true values, θ_s and θ_v. The light green side-lines around the estimates reflect the $\pm 3\sigma$ range for the estimated mean given the estimator's covariance matrix.

F. Extension to 3D Stabilization with Moving Anchor Point

The planar approach described above was extended to stabilize all the degrees of freedom of the vehicle except for yaw: two separate instances of the estimator and the controller were run for each of the two vertical planes: one for (x_g, z_g) and another one for (y_g, z_g). We ignore any coupling effects between the dynamics in the two planes, but increase τ_s to 1.2 s and ζ_s to 0.8 to improve robustness. The estimators and controllers operator on project vertical-plane force components, projected at each time step using the currently estimated attitude.

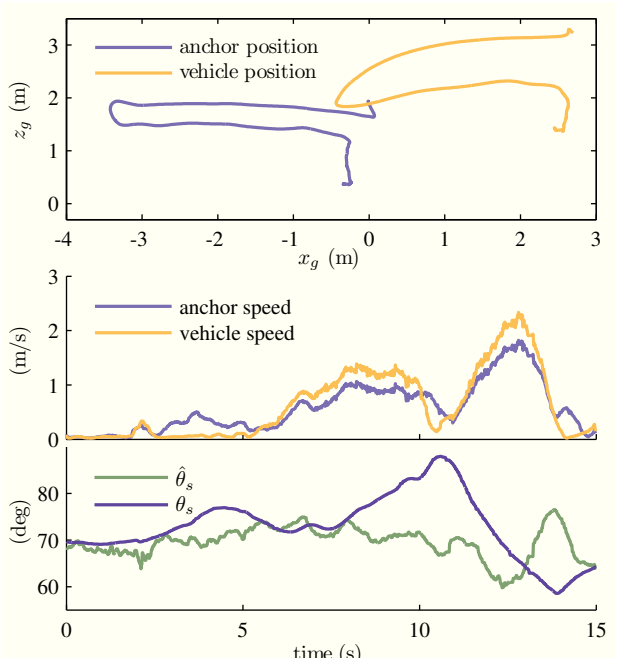

Fig. 11. Tethered vehicle stabilizing as the anchor point is shifted. The top plot shows the movement of the anchor point and the vehicle; the corresponding velocities are shown in the middle plot. The bottom plot shows the estimated tether angle and the actual tether angle.

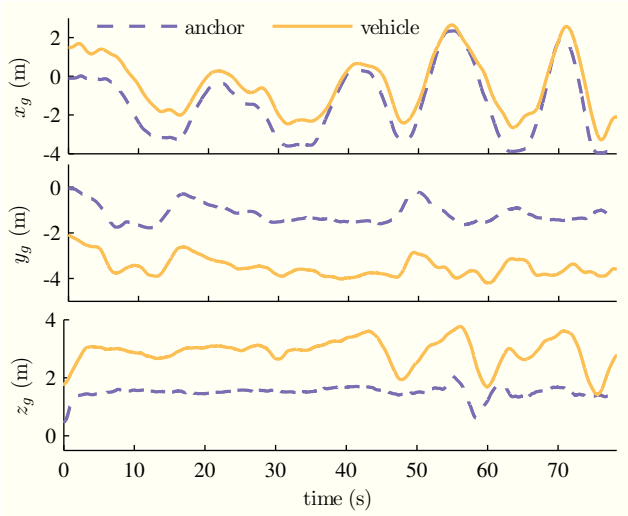

Fig. 12. Vehicle stabilizing in 3D relative to a moving anchor point.

The experiment of the vehicle stabilizing relative to the anchor point was repeated with this setup. Results are shown in Fig. 12. The vehicle was observed to stabilize, though with a significant tether angle bias. Further work to properly estimate and model coupled 3D dynamics is necessary to remove the bias and achieve higher-performance stabilization.

VIII. Conclusions and Future Work

The 2D dynamics of a hover-capable UAV attached to a fixed point by a taut tether were presented along with a method to recover the force induced by the tether and the angles of the tether and of the vehicle, using only minimal on-board inertial sensors. A state estimation and control scheme were presented. Importantly, the proposed localization is purely relative to the fixed ground point of the

tether, allowing for intuitive lateral shifting of the nominal vehicle position by shifting the anchor point, using the normal control/localization approach in a quasistatic manner.

The sensitivity of the localization method to sensor noise and to vehicle non-idealities was analyzed for sample realistic scenarios. Initial experiments demonstrated the proposed localization, estimation, control and interaction schemes.

As this work was an initial study of this type of system, a number of improvements can be implemented for the localization scheme. Currently, the vehicle operates in a vertical plane – preliminary results showed that the same approach yields stable control in 3D, by assuming that (x_g, z_g) dynamics are decoupled from (y_g, z_g) dynamics. However the resulting systems performance is relatively poor, suggesting that significant coupling needs to be considered.

Further sensors on the vehicle can significantly improve the estimator. Specifically, a linear or directional force sensor can be used at the tether-vehicle attachment point to directly observe F_s, $(\theta_s - \theta_v)$, and yaw. A rate gyro can be installed directly on the tether to measure $\dot{\theta}_s$.

Similar methodologies may be applicable to non-flying systems such as buoyant or suspended/swinging systems. For aerial vehicles, in addition to the localization and interaction benefits described herein, a tether provides additional significant benefits in terms of increasing safety and meeting regulations. Taut-tethered hover-capable UAVs offer solutions to the fundamental problems faced by free-flying UAVs and as a result may enable new application areas for aerial systems.

ACKNOWLEDGMENTS

The authors thank Markus Hehn for the discussions relating to this work. We also thank Mark Müller for his UKF implementation. Experiments presented in this work were performed in the ETH Zurich Flying Machine Arena, built by contributors listed in `tiny.cc/FMApeople`.

This research was supported in part by the Swiss National Science Foundation through both the National Centre of Competence in Research Robotics and through direct grants to the Institute for Dynamic Systems and Control.

APPENDIX I
LINEARIZED PLANT

We may rewrite the plant dynamics described in Section II in canonical state-space linearized form as follows, with input $u = \dot{\theta}_v^*$ and state $\mathbf{x} = \left(\theta_s, \dot{\theta}_s, \theta_v, \dot{\theta}_v, \ddot{\theta}_v\right)$:

$$\dot{\mathbf{x}} = \mathbf{A}\mathbf{x} + \mathbf{B}u \tag{22}$$

where, given $\gamma = \cos(\theta_s - \theta_v)$,

$$\mathbf{A} = \begin{bmatrix} 0 & 1 & 0 & 0 & 0 \\ \frac{g\cos\theta_s - F_p\gamma}{l} & 0 & \frac{F_p}{l}\gamma & 0 & 0 \\ 0 & 0 & 0 & 1 & 0 \\ 0 & 0 & 0 & 0 & 1 \\ 0 & 0 & 0 & -\omega_{vd}^2 & -2\zeta_{vd}\omega_{vd} \end{bmatrix} \tag{23}$$

and

$$\mathbf{B} = \begin{bmatrix} 0 & 0 & 0 & 0 & \omega_{vd}^2 \end{bmatrix}^T \tag{24}$$

APPENDIX II
LINEARIZED CONTROLLER

For a given operating point, $\breve{\mathbf{x}} = (\breve{\theta}_s, 0, \breve{\theta}_v, \cdot, \cdot)$ we may linearize the control law described in Section V as:

$$u = \frac{1}{\tau_v} \begin{bmatrix} 1 - (l/\tau_s^2 + g\cos(\theta_s^*))/\alpha \\ -2\zeta_s l/(\tau_s \alpha) \\ -1 \\ 0 \\ 0 \end{bmatrix}^T (\mathbf{x}^* - \mathbf{x}) \tag{25}$$

where

$$\alpha = F_p^* \sqrt{1 - \left(\frac{2\zeta_s l \dot{\theta}_s^*}{\tau_s} + g\sin(\theta_s^*)\right)^2 / F_p^{*2}} \tag{26}$$

Note that the state has five elements – however the last two are not observed by the localization or the estimator and reflect underlying dynamics.

REFERENCES

[1] S. Weiss, D. Scaramuzza, R. Siegwart, Monocular-SLAM-based navigation for autonomous micro helicopters in GPS-denied environments, J. Field Robot. 28 (6) (2011) 854–874. doi:10.1002/rob.20412.

[2] M. Achtelik, A. Bachrach, R. He, S. Prentice, N. Roy, Stereo vision and laser odometry for autonomous helicopters in GPS-denied indoor environments, in: Proceedings of the SPIE Unmanned Systems Technology XI, Vol. 7332, Orlando, F, 2009. doi:10.1117/12.819082.

[3] Cyphy works, `http://cyphyworks.com/` (Accessed 01.2013).

[4] N. N. White, Evolution of the design and modeling of the eagle system, Masters thesis, Case Western Reserve University (2011).

[5] C. Hardham, Tethered system for power generation, WO Patent WO/2010/134,997 (2010).

[6] P. McKerrow, D. Ratner, The design of a tethered aerial robot, in: Robotics and Automation, 2007 IEEE International Conference on, 2007, pp. 355 –360. doi:10.1109/ROBOT.2007.363812.

[7] S.-R. Oh, K. Pathak, S. Agrawal, H. Pota, M. Garratt, Approaches for a tether-guided landing of an autonomous helicopter, Robotics, IEEE Transactions on 22 (3) (2006) 536–544. doi:10.1109/TRO.2006.870657.

[8] F. Muttin, Umbilical deployment modeling for tethered UAV detecting oil pollution from ship, Applied Ocean Research 33 (4) (2011) 332 – 343. doi:10.1016/j.apor.2011.06.004.

[9] P. Abad-Manterola, J. Edlund, J. Burdick, A. Wu, T. Oliver, I. Nesnas, J. Cecava, Axel, Robotics & Automation Magazine, IEEE 16 (4) (2009) 44–52. doi:10.1109/MRA.2009.934821.

[10] A. Mozas-Calvache, J. Prez-Garca, F. Cardenal-Escarcena, E. Mata-Castro, J. Delgado-Garca, Method for photogrammetric surveying of archaeological sites with light aerial platforms, Journal of Archaeological Science 39 (2) (2012) 521 – 530. doi:10.1016/j.jas.2011.10.007.

[11] P. Martin, E. Salaun, The true role of accelerometer feedback in quadrotor control, in: Robotics and Automation (ICRA), 2010 IEEE International Conference on, 2010, pp. 1623 –1629. doi:10.1109/ROBOT.2010.5509980.

[12] S. Lupashin, A. Schöllig, M. Sherback, R. D'Andrea, A simple learning strategy for high-speed quadrocopter multi-flips, in: Robotics and Automation (ICRA), 2010 IEEE International Conference on, 2010, pp. 1642 –1648. doi:10.1109/ROBOT.2010.5509452.

[13] S. J. Julier, J. K. Uhlmann, Unscented filtering and nonlinear estimation, Proceedings of the IEEE 92 (3) (2004) 401–422. doi:10.1109/JPROC.2003.823141.

[14] Y. Bar-Shalom, T. Kirubarajan, X.-R. Li, Estimation with Applications to Tracking and Navigation, John Wiley & Sons, Inc., New York, NY, USA, 2002.

[15] W. Wonham, On the separation theorem of stochastic control, SIAM Journal on Control 6 (2) (1968) 312–326. doi:10.1137/0306023.

[16] K. Xiong, H. Zhang, C. Chan, Performance evaluation of ukf-based nonlinear filtering, Automatica 42 (2) (2006) 261 – 270. doi:10.1016/j.automatica.2005.10.004.